

Weathering of ilmenite from granite and chlorite schist in the Georgia Piedmont

PAUL A. SCHROEDER,* JOHN J. LE GOLVAN, AND MICHAEL F. RODEN

Department of Geology, University of Georgia, Athens, Georgia 30602-2501, U.S.A.

ABSTRACT

Ilmenite grains from weathering profiles developed on granite and ultramafic chlorite schist in the Georgia Piedmont were studied for evidence of morphological and chemical alteration. Ilmenite-rich concentrates from the fine sand (90–150 μm) component were studied to test the assumption that there is no difference between ilmenite in the parent rock and that in colluvium delivered to primary drainage systems.

Ilmenite grains in the granite profile are rounded to subhedral, and commonly contain hematite exsolution blebs. Dissolution pits are observed along the boundaries of the exsolution blebs, with goethite occurring as an alteration product. Ilmenite grains in the schist profile occur as fractured anhedral grains with uncommon lamellae of rutile. Grain fractures are filled with goethite and hematite, particularly in the B-horizon. Ilmenite from the granite profile is Mn rich (7–15 mol% MnTiO_3), whereas ilmenite from the schist profile contains only 1–2 mol% MnTiO_3 and up to 8 mol% MgTiO_3 . Two populations of grains develop in both profiles. Grains with abundant exsolution blebs and fractures alter through a proposed two-step reaction mechanism. It is proposed that ilmenite first undergoes a solid-state transformation to pseudorutile via an anodic oxidation mechanism. Oxidized Fe and Mn diffuse from the structure and precipitate as goethite and MnO_2 . Pseudorutile is ephemeral and undergoes incongruent dissolution to form anatase, hematite, and goethite. The second population of grains experienced only slight oxidation and dissolution on grain surfaces, and they persist through the weathering profile. The Fe^{2+} content of competent ilmenite grains is somewhat lower in the C-horizon, compared with grains in the host rock. In horizons above the C-horizon, the Fe^{2+} contents of the ilmenite are similar to those in the host rock.

This study shows that using ilmenite minor-element chemistry as a tracer for sediment provenance is a valid technique, however, textural features of ilmenite in colluvium may be distinct from those in the parent rock. Also, the production of secondary phases, such as anatase, goethite, and hematite, in soil profiles results in part from the alteration of ilmenite.

INTRODUCTION

The crystal chemistry of ilmenite has been studied in support of a wide array of geochemical interests. For example, ilmenites coexisting with magnetite-ulvospinel solid solutions have provided petrologists with information on the oxygen fugacity and temperature at which magmas crystallize (Buddington and Lindsley 1964). Ilmenite is also a principal heavy mineral in clastic sedimentary rocks and has been used to trace the origin of sandstones (Basu and Molinaroli 1989; Puffer and Cousminer 1982; Schneiderman 1995; Grigsby 1990, 1992; Darby 1984; Darby and Tsang 1987). Ilmenite and associated Ti minerals in ancient strandlines constitute economic deposits that are of importance to metal alloy and pigment industries (Force 1991; Bailey et al. 1956). The alteration of ilmenite in soil environments has received nowhere the same attention as ilmenite studied in the context of igneous, metamorphic, and sedimentary environments (Anand and Gilkes 1984; Cornu et al. 1999; Dimanche and Bartholomé 1976; Frost

et al. 1983, 1986; Lynd 1960). The purpose of the present study is to evaluate the chemical and textural properties of ilmenite in the weathering profiles developed on crystalline bedrock in a temperate to subtropical climate. The intent is to provide further insights into the role of ilmenite in pedogenesis and to determine the extent of crystal-chemical modifications that occur during weathering.

METHODS

Sample sites and processing

Two regoliths from ridge crest sites on crystalline basement in the Georgia Piedmont were selected with the intention of obtaining wholly residual weathering profiles. The first site is situated on the Elberton Granite in the Keystone Quarry, 5 km south of Elberton, GA (34° 3.97'N, 82° 50.15'W, 183 m elevation). The Elberton Granite is a large (~500 km²), fine-grained granite composed of alkali feldspar, plagioclase, quartz, biotite, and minor amounts of ilmenite, magnetite, sphene, allanite, and zircon (Stormer et al. 1980). This granite was chosen because it represents a parent rock of felsic composition with a rela-

* E-mail: schroe@uga.edu

tively homogeneous composition and texture. The parent granite (PR), a core stone (CS), saprolite (C-horizon), C1-, BC-, Bt₁-, Bt₂-, and AB-horizons were sampled from exposed quarry walls, where the regolith averages about 11 m in thickness. The A-horizon was not sampled due to disruption associated with quarry operations. The soil is classified as a fine, kaolinitic, thermic Typic Kanhapludult (Hamilton-Wood 2002).

The second site is situated on the Shoulderbone chlorite schist located 10 km northwest of Sparta, GA (33° 20.49'N, 83° 4.80'W, 133 m elevation). This schist is one of numerous small ultramafic bodies of uncertain origin that occur within Piedmont metamorphic rocks of Georgia and the Carolinas (Misra and Keller 1978). The rock is foliated in places, which could cause minor heterogeneity in mineral abundance. The soil is classified as a fine, mixed, superactive, thermic Typic Hapludalf (Hamilton-Wood 2002). The regolith averages about 1 m thick, therefore, variations due to parent rock in the profile are assumed minimal. Bulk densities for all samples were determined using the standard ring-insertion method (Blake and Hartge 1986) and a Jolly balance.

Approximately 1.5 kg of bulk material was selected for homogenization. Indurated samples were powdered to <20 µm with a percussion mortar. A split of each sample was sent to XRAL Laboratories located in Don Mills, Ontario, Canada for determination of loss-on-ignition (LOI) and elemental analysis by X-ray fluorescence (XRF) methods. The remaining split was mildly dispersed using a hydrogen peroxide treatment (to remove labile organic matter) and ultra-sonification with sodium metaphosphate (added as a dispersant). All samples were subsequently wet-sieved to isolate the 90–150 µm fraction (herein referred to as fine sand). This size range was selected because it overlaps the very-fine and fine sand fractions traditionally used by sedimentologists. This fraction should survive transport in colluvial, fluvial, and aeolian environments and be preserved in sedimentary rocks.

The highly magnetic fine sand was removed by passing a bar magnet over the sample. The remaining fraction was passed through a Frantz Isodynamic Separator configured at 15° front tilt, 25° side tilt, and 0.4 amperes current (Flinter 1959a, 1959b). Elberton samples required additional separation because biotite occurred as a major constituent of the magnetic separate. Small amounts of sample were poured onto the edge of filter paper. Tilting and shaking the paper resulted in retardation of mica movement, while the non-micaceous minerals rolled off. Optical examination of the two separate fractions revealed efficient removal of micas.

Analytical techniques

The magnetic separates were split for X-ray diffraction (XRD) and microprobe analysis. XRD samples were ground using a boron-carbide mortar and pestle and then slurried with ethyl alcohol onto a zero-background quartz plate. XRD analysis was performed on a Scintag XDS 2000 diffractometer, using CoK α radiation. Data were collected over the range of 10 to 80 °2 θ , using a step increment of 0.01 °2 θ , with a count time of 6 s/step. Corundum (15% by weight) was added as an internal standard for some of the analyses.

Polished epoxy grain mounts were carbon coated for wave-

length-dispersive spectroscopy (WDS) electron microprobe analysis using a JEOL JXA-8600 Superprobe. Beam current was 15 nA and accelerating voltage was 15 kV. The ϕ - ρ -Z matrix correction of Bastin et al. (1984) was employed for the calculation of oxide abundance. Grains were analyzed for Fe, Ti, Mg, Mn, Ni, Al, Cr, Ca, and Si using natural and synthetic mineral standards.

RESULTS

Bulk properties of weathering profiles

Oxide analyses and bulk densities for samples from the Elberton and Shoulderbone regoliths are presented in Tables 1 and 2, respectively. Our analysis (column 1, Table 1) of the Elberton Granite is similar to the average analysis reported by Stormer et al. (1980); they note that the Elberton Granite is similar to that of average granite (LeMaitre 1976). The Elberton Granite mineral assemblage consists of quartz, microcline, plagioclase, biotite, hematite, ilmenite, and magnetite, as evidenced by XRD data and previous work by Stormer et al. (1980). Secondary phyllosilicates that appear in the A- and B-horizons include halloysite, kaolinite, and hydroxy-interlayered-vermiculite (HIV). Oxides identified include anatase, hematite, and goethite.

The Shoulderbone schist (column 1, Table 2) is rich in MgO and Fe₂O₃(T). The moderate SiO₂ content combined with the high MgO and Fe₂O₃(T) and relatively low CaO suggest that the original protolith was dominated by orthopyroxene and olivine, and that the rock was a relatively Fe-rich (Mg no. = 74.4) harzburgite. The Shoulderbone schist mineral assemblage consists of clinocllore, anthophyllite, actinolite/tremolite, ilmenite, magnetite, quartz, olivine, and rutile. The abundant anthophyllite in the rock is consistent with the harzburgite protolith hypothesis, because anthophyllite forms by reaction between orthopyroxene and metamorphic fluids (Deer et al. 1992). The high Si values relative to a basaltic rock suggest,

TABLE 1. Weight percent oxide analysis and density values for bulk material from the Elberton granite weathering profile

Oxide	Horizon (depth cm)						
	bedrock (1100)	CS* (800)	C (600)	BC (282)	Bt ₂ (172)	Bt ₁ (132)	AB (40)
SiO ₂	70.60	71.40	70.30	71.80	71.10	65.90	81.70
Al ₂ O ₃	14.20	13.70	16.20	15.00	15.70	22.20	9.44
CaO	1.69	1.66	0.24	0.28	0.04	0.86	0.13
MgO	0.60	0.64	0.53	0.49	0.46	0.03	0.49
Na ₂ O	3.16	2.85	0.73	0.83	0.32	0.04	0.10
K ₂ O	5.23	4.63	5.73	5.88	5.86	0.82	2.28
Fe ₂ O ₃	2.55	2.90	2.65	2.43	2.44	1.72	2.01
MnO	0.04	0.04	0.05	0.03	0.03	0.00	0.03
TiO ₂	0.36	0.40	0.38	0.34	0.34	0.16	0.65
P ₂ O ₅	0.10	0.10	0.04	0.03	0.04	0.08	0.02
Cr ₂ O ₃	0.04	0.03	0.03	0.03	0.04	0.03	0.04
LOI†	0.30	0.90	3.35	3.50	3.30	8.30	3.00
Total	98.87	99.25	100.23	100.64	99.67	100.14	99.89
Bulk density	2.70	2.55	2.50	1.50	1.39	1.26	1.52
g/cm ³							
% Porosity	0	6	7	44	49	54	44
Strain factor‡	0.00	-0.05	0.01	0.89	1.06	3.84	-0.02

* Core stone.

† Loss on ignition. Assumed to represent H₂O in analysis of mass transfer functions.

‡ Value of ϵ calculated relative to the parent rock using Equation 2 assuming Ti is a conservative component.

TABLE 2. Weight percent oxide analysis and density values for bulk material from the Shoulderbone weathering profile

Oxide	Horizon (depth cm)						
	bedrock (170)	C ₁ (140)	C ₂ (78)	BC (60)	Bt ₂ (50)	Bt ₁ (30)	A (5)
SiO ₂	49.10	43.90	45.70	43.80	44.00	44.30	45.50
Al ₂ O ₃	5.74	6.27	6.65	8.76	7.87	6.34	6.16
CaO	3.30	3.46	3.27	2.01	2.65	3.34	1.93
MgO	21.60	21.00	20.50	18.20	18.50	21.40	19.60
Na ₂ O	0.39	0.26	0.26	0.16	0.20	0.25	0.14
K ₂ O	0.06	0.07	0.05	0.08	0.09	0.07	0.12
Fe ₂ O ₃	14.70	17.30	16.60	18.60	19.30	16.90	16.60
MnO	0.21	0.21	0.22	0.22	0.24	0.29	0.41
TiO ₂	1.03	1.96	0.92	1.06	0.84	1.29	1.36
P ₂ O ₅	0.10	0.05	0.04	0.06	0.07	0.07	0.13
Cr ₂ O ₃	0.17	0.13	0.14	0.15	0.14	0.18	0.15
LOI*	3.75	5.55	5.40	6.45	6.20	5.20	8.00
Total	100.15	100.16	99.75	99.55	100.10	99.63	100.10
Bulk density g/cm ³	2.93	2.66	2.55	2.43	2.35	2.15	1.58
% Porosity	0	9	13	17	20	27	46
Strain factor†	0.00	-0.42	0.29	0.18	0.52	0.09	0.42

* Loss on ignition. Assumed to represent H₂O in analysis of mass transfer functions.

† Value of ϵ calculated relative to the parent rock using Equation 2 assuming Ti is a conservative component.

that during prograde metamorphism there was an influx of Si. Secondary minerals, halloysite, kaolinite, anatase, hematite, and goethite appear in the A- and B-horizons.

Ilmenite textural and chemical properties

Twenty five grains from each horizon were analyzed. For each grain, a core and rim analysis was performed. Student's two-tailed t-tests were performed on selected populations of the data set to determine if significant differences between the core and rim compositions are present. The intent was to identify oxidative weathering fronts that may have propagated from the outside to the inside of the grains. In most cases there are slightly lower Fe contents in the core region (Fig. 1). However, the difference between core and rim are small and most of the t-tests did not show a significant difference between the analyses at the $\alpha = 0.05$ confidence level. This indicates that ilmenite zoning is typically negligible.

Ilmenite from the Elberton Granite occurs as rounded to subhedral grains and contains minor amounts of MnTiO₃ and Fe₂O₃ (Table 3) as is typical of ilmenites from granites (e.g., Haggerty 1976). Included blebs of hematite are very common. Reflected light microscopy reveals a subpopulation of ilmenite grains in the core stone that have slightly lower reflectance (Fig. 2a), but no red internal reflections (red being indicative of included hematite). In the C-horizon, ilmenite grains show red hematite replacement textures, as well as diminished reflectance. Grains from the B-horizon exhibit significant alteration to hematite. Altered hematite-rich grains are uncommon in the AB-horizon, suggesting that they have either dissolved or the AB horizon never contained the highly altered ilmenite grains.

A second subpopulation of competent ilmenite grains from the Elberton site persists throughout the weathering profile. In back-scattered electron (BSE) images, these grains appear homogeneous. Optical microscopy, however, revealed hematite exsolution lamellae in these grains. The inability to distinguish

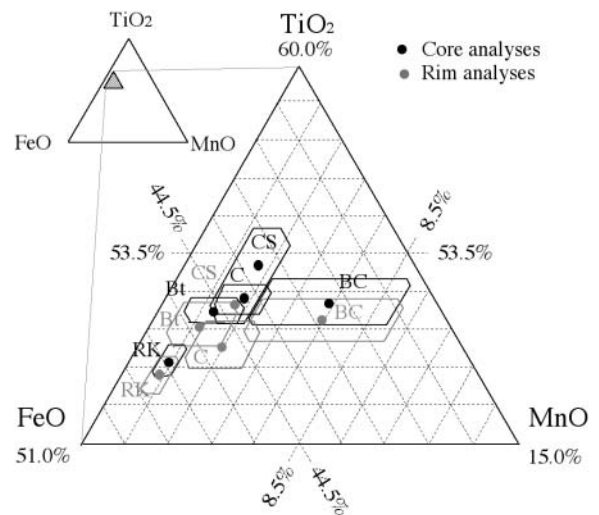


FIGURE 1. TiO₂-FeO-MnO ternary diagram comparing of Elberton Granite ilmenite grain core compositions (black circles) with rim compositions (gray circles). Hexagonal polygons outline standard deviation ($\sigma = 1$), with $n = 25$ for each population. RK = Bedrock. See Table 3 for other horizon symbol codes.

TABLE 3. Average* weight percent oxide analysis and structural formulae of ilmenite grains from the Elberton Granite weathering profile.

Oxide	Horizon (depth cm)					
	bedrock (1100)	CS† (800)	C (600)	BC (282)	Bt (172)	AB‡ (40)
SiO ₂	0.04	0.03	0.00	0.01	0.04	—
TiO ₂	48.55	51.14	49.65	50.08	50.58	—
Cr ₂ O ₃	0.00	0.00	0.00	0.00	0.00	—
FeO	46.21	42.23	43.27	40.28	44.39	—
MnO	3.04	3.96	4.32	6.86	3.61	—
MgO	0.05	0.07	0.05	0.09	0.14	—
CaO	0.07	0.03	0.01	0.01	0.00	—
NiO	0.00	0.00	0.00	0.00	0.00	—
Total	97.96	97.46	97.30	97.33	98.76	—
Fe ₂ O ₃ §	5.96	0.00	2.87	1.58	2.65	—
Cation§						
Ti	0.98	1.00	0.99	0.99	0.99	—
Fe ³⁺	0.06	0.00	0.03	0.02	0.03	—
Fe ²⁺	0.92	0.92	0.90	0.86	0.92	—
Mn	0.06	0.08	0.09	0.14	0.07	—
Mg	0.00	0.00	0.00	0.00	0.01	—

* $n = 50$ individual analyses per horizon.

† Core stone.

‡ Ilmenite grains from this horizon were not analyzed due to sampling uncertainties.

§ See text for method of recalculation. Cations on the basis of three oxygen per unit formula.

hematite from ilmenite with BSE imaging, makes it difficult to select pure sites for WDS analysis.

Ilmenite from the Shoulderbone site occurs as anhedral grains (Fig. 3a) and contains minor and variable amounts of MnTiO₃ and MgTiO₃. Table 4 shows the average ($n = 50$ per horizon) compositions for ilmenites from the Shoulderbone profile. In the cases of ilmenite from the parent rock and the C-horizon, small amount of negative Fe³⁺ values were calculated.

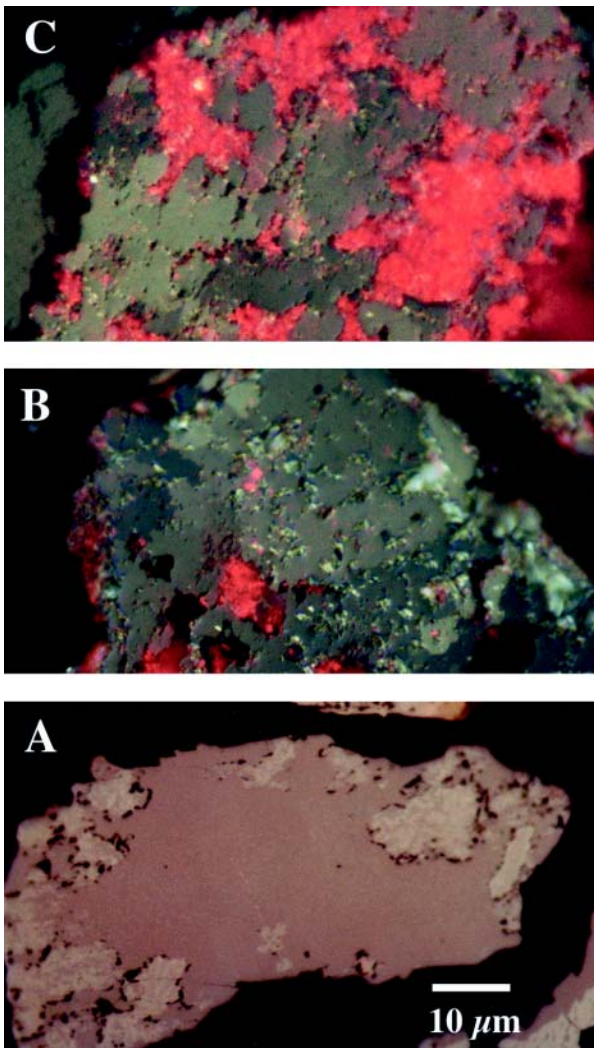


FIGURE 2. Reflected light photomicrographs (all at same scale) of ilmenite grains from the Elberton Granite. (A) Grain from a core stone with ilmenite showing as light pink reflectance and hematite blebs appearing with a much lighter reflectance. (B) Grain from a core stone with ilmenite showing lower reflectance and faint red internal reflections. Hematite replaces ilmenite and hematite blebs show strong red internal reflections. (C) Altered grain from the B-horizon shows hematite replacement of ilmenite. Reflectance of the remaining ilmenite, is much lower than unaltered ilmenite and large patches of hematite red internal reflections are visible.

This result is an artifact of excess TiO_2 caused by a small amount of rutile exsolution and analytical error.

The relatively high MgTiO_3 content of ilmenite in the parent rock is typical of ilmenites from mafic and ultramafic plutonic rocks (Haggerty 1976) and distinguishes these ilmenites from those of the parent Elberton Granite. Lamellae or inclusions are rare and, where present, appear as thin rutile zones. Ilmenite in the parent rock appears both as structurally intact grains and as highly fractured grains (Fig. 3b). Some grains have internal dissolution pits, possibly due to dissolution of silicate inclusions. In the weathering profile,

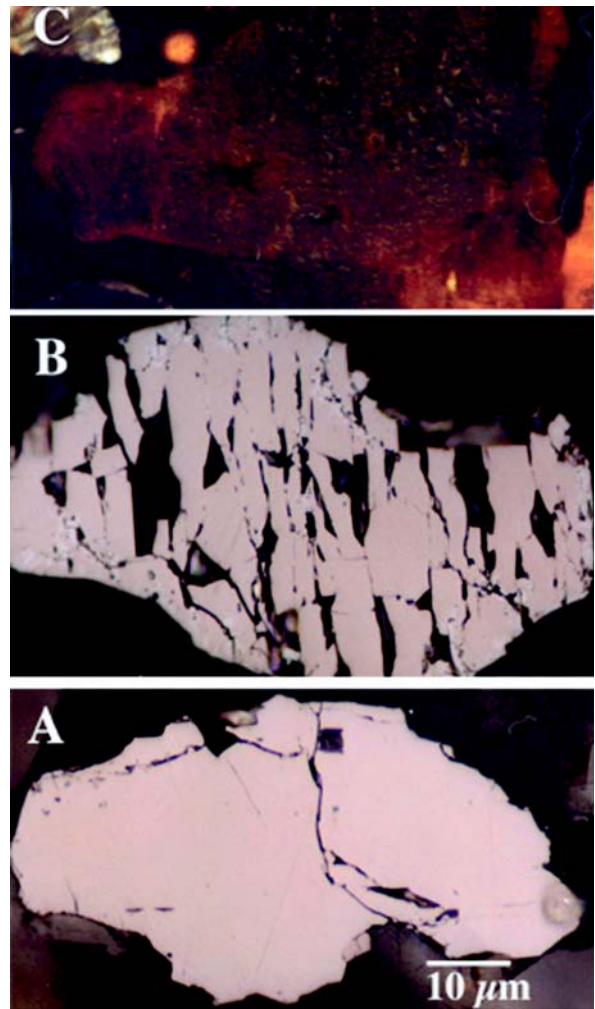


FIGURE 3. Reflected light photomicrographs (all at same scale) of ilmenite grains from the Shoulderbone schist. (A) Unaltered ilmenite grain from the C-horizon with brighter reflectance than unaltered Elberton Granite ilmenite grains. (B) Weathered and fractured grain from the B-horizon with ilmenite showing lower reflectance. (C) Altered grain from the A-horizon shows the remaining ilmenite is much lower than unaltered ilmenite. Pervasive yellow internal reflections are micropores of goethite.

grain fractures are filled with small amounts of hematite and goethite in some cases (Fig. 3c). As in the granite weathering profile, the ilmenite grains from the schist occur in two subpopulations. One set appears progressively more altered proceeding up the profile, while a second set appears intact into the A-horizon. No attempts were made to assess the relative proportion of grain populations; however, the relative peak heights of the hematite (024) and ilmenite (024) XRD reflections in the Frantz separate indicate the proportion of hematite relative to ilmenite increases up the profile.

TABLE 4. Average* weight percent oxide analysis and structural formulae of ilmenite grains from the Shoulderbone schist weathering profile

Oxide	Horizon (depth cm)						
	bedrock (170)	C ₁ (140)	C ₂ (78)	BC (60)	Bt ₂ (50)	Bt ₁ (30)	A (5)
SiO ₂	0.36	0.01	0.02	0.03	0.02	0.02	0.00
TiO ₂	52.74	52.46	51.59	51.60	51.45	51.30	51.35
Cr ₂ O ₃	0.01	0.06	0.08	0.11	0.05	0.11	0.10
FeO	44.22	44.93	44.21	44.15	42.82	44.32	44.80
MnO	0.97	0.89	0.50	0.53	0.58	0.67	0.79
MgO	0.19	0.26	2.18	2.18	1.92	1.33	0.79
CaO	0.02	0.01	0.06	0.03	0.04	0.04	0.01
NiO	0.00	0.01	0.06	0.00	0.00	0.00	0.00
Total	98.51	98.63	98.70	98.63	96.88	97.79	97.84
Fe ₂ O ₃ [§]	-2.23	-1.10	2.38	0.99	0.57	1.28	0.81
Cation [§]							
Ti	1.01	1.00	0.99	0.99	1.00	1.00	1.00
Fe ³⁺	0.00	0.00	0.03	0.02	0.00	0.00	0.01
Fe ²⁺	0.98	0.98	0.90	0.90	0.91	0.93	0.95
Mn	0.02	0.02	0.01	0.01	0.01	0.01	0.02
Mg	0.01	0.01	0.08	0.08	0.07	0.05	0.03

* *n* = 50 individual analyses per horizon.

† See text for method of recalculation. A negative value indicates excess TiO₂ (i.e., rutile exsolution) and no excess FeO correction made. Cations on the basis of 3 oxygen per unit formula.

DISCUSSION

Changes in bulk properties

The textural and chemical properties of fine sand ilmenite grains observed in the weathering profiles provide an opportunity to assess how earth-surface processes might modify ilmenite chemistry. The properties of ilmenite grains, as they are set by igneous and metamorphic conditions, require consideration. Basu and Molinaroli (1989) noted that a wide range of textures in Fe-Ti oxides are possible depending upon subsolidus reactions in igneous rocks as they cool through various ranges of temperatures and oxygen fugacity. This variability is seen where the ilmenite grains found in the granite have a greater number of hematite inclusions than the ilmenite grains found in the ultramafic schist. The extent to which ilmenite incorporates minor elements in high-temperature igneous and metamorphic systems is a function of bulk composition and the nature of co-precipitating phases. In the Elberton Granite, Mn is the only minor element substituting in ilmenite (Table 3) whereas in the Shoulderbone schist both Mg and Mn substitute in the ilmenite. These distinctions result from the large differences in the bulk composition of the granite and the schist (Tables 1 and 2). Furthermore, Frost and Lindsley (1992) have shown that ilmenite grains with a high amount of Cr are commonly derived from ultramafic rocks emplaced into ocean crust. The low Cr content of the Shoulderbone ilmenite grains therefore suggests that its ultramafic protolith was not from within ocean crust.

When considering the stoichiometry of ilmenite in these two parent rocks, the ability to discriminate the provenance of sediment derived from these rocks appears quite valid. However, textural and related chemical modifications might occur in ilmenite while exposed to an acidic, temperate to subtropical climatic weathering regime that potentially can complicate

provenance studies. Understanding the pathways for ilmenite grain modification as a function of weathering regime is also important for establishing the origin of secondary alteration products in soil/saprolite and, hence, minerals that are potentially preserved in paleosols. The tacit assumption made in many soil studies is that weathering profiles can be treated as one-dimensional reaction fronts propagating into the landscape. It is also assumed that the profiles developing today have been derived from parent rock that is homogeneous in composition.

The most common approach to quantifying solid-state mass losses, indicative of long-term weathering rates, is to determine the mass-transfer coefficients (τ_i) for elemental species across successive unit volume horizons (where *i* is the species of interest). This approach employs the mobility of elements relative to an assumed conservative species (*j*) such as Ti (Brimhall and Dietrich 1987; Merritts et al. 1992; White et al. 1998). Equation 1 depicts the relationship between τ_i and the concentration (*C*) of a species in the parent rock (*p*) and in weathering horizons (*w*), the density (ρ), and volume (*V*) changes described by a strain factor, ϵ , where $\epsilon = V\alpha / V\beta - 1$ (Eq. 2). *V* α and *V* β are the volumes of parent rock and any general weathered material in the section. τ and ϵ are ratios. There are no units on them.

$$\tau_j = \frac{\rho_w C_{j,w}}{\rho_p C_{j,p}} (\epsilon_{j,w} + 1) - 1 \quad (1)$$

where,

$$\epsilon_j = \frac{\rho_j C_{i,p}}{\rho_w C_{i,w}} - 1 \quad (2)$$

If $\tau_i = -1$, then the species is completely lost from the system. If $\tau_i = 0$, then *i* is conserved and only affected by closed system processes. If $\tau_i > 0$, then an excess mass of the oxide species is present relative to the parent rock. Gardner (1980) has noted that in some environments, Ti can be mobile; however, in the moderately acidic temperate climates, the assumption of Ti immobility is reasonable for first-order evaluations (Chadwick et al. 1990). Elemental mass-transfer fractions of the major oxides were calculated with the data in Table 1 and 2 using Equations 1 and 2 and are graphically presented for the Elberton and Shoulderbone sites in Figures 4 and 5 respectively.

Figure 4 shows Mg, Na, and Ca are lost from the Elberton profile, whereas Fe, Al, and H experience gains. Si appears to be relatively conservative within the system. Calcium, Si, Fe, Al, and H exhibit positive excursions in the B-horizon. Mass transfer from the A-horizon to the B-horizon via dissolution/precipitation reactions and/or translocation of clay minerals can result in a positive τ_i excursion. The slight positive excursion of Ca in the B-horizon is at first perplexing if an external input of material is not considered.

Two sources of Ca are possible. It is possible that recent quarry activity has added a component of fresh granite to the land surface. Dissolution of plagioclase provides a source of Ca that would be preferentially adsorbed by hydroxy-interlayered vermiculite under dilute solute conditions (Berner 1980). The slight increase in P content in the B-horizon sug-

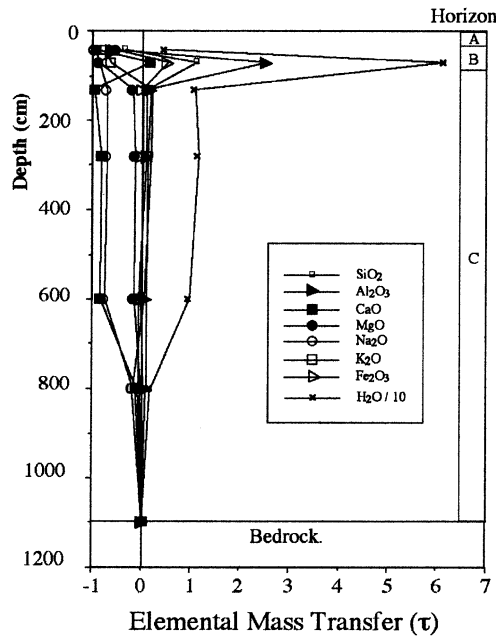


FIGURE 4. Weathering characteristics as a function of depth in the Elberton Granite regolith as defined by Equation 1. Elemental mass transfer, τ_i , is calculated such that -1.0 is equivalent to total loss, and zero is no loss relative to TiO_2 in the parent rock.

gests a relative increase in apatite content, which could also contribute Ca to the bulk chemistry. Another origin for the Ca gain is eolian or fluvial input from above. Consistent with the above idea, is the occurrence of small amounts of epidote and hornblende found in the B-horizon, which suggests a metamorphic component derived from the regionally metamorphosed country rock.

All elements, except Al, in the Shoulderbone profile display mass losses in the transition from the parent rock to the C-horizon (Fig. 5). The apparent initial loss of H reflects congruent dissolution of the amphiboles or it may be a consequence of an initially lower Ti abundance in the parent rock at that point in the profile. A second possible explanation for the negative H trend is may be that it is an artifact from the LOI trend, which includes gaining of O_2 upon heating to 925°C and the conversion of FeO to Fe_2O_3 . Net gains of Fe, K, Al, and H seen in the B-horizon, are attributed to formation of clay minerals and oxyhydroxide precipitation and translocation. All elements, except K and H, exhibit losses from the B- to the A-horizon. The mass loss is a response due to dissolution and translocation mechanisms, similar to that seen in the Elberton profile.

The positive excursions of τ_K and τ_H are attributed to an increase in organic matter content. In this case the LOI value includes an organic matter component (i.e., $\text{LOI} = \text{H}_2\text{O} + \text{CH}_2\text{O}$, and changes due to FeO oxidation). The increased τ_K value reflects an external input associated with forest floor nutrient cycling phenomena and possible wind-blown micas from the adjacent metamorphic terrain (Schroeder et al. 1997).

In the case of the Elberton Granite, the lower exposure of the quarry wall reveals ~ 7 meters of equigranular saprolitic granite. An assumption of isovolumetric weathering appears to be valid because the textures are unchanged. The bulk chemistry data of

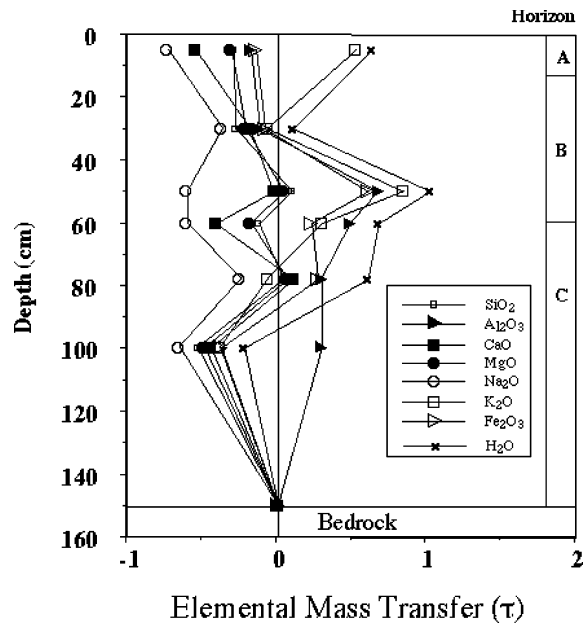


FIGURE 5. Weathering characteristics as a function of depth in the Shoulderbone schist regolith as defined by Equation 1. Elemental mass transfer τ_i is calculated such that -1.0 is equivalent to total loss and zero is no loss relative to TiO_2 in the parent rock.

the Elberton A- and B₁-horizons (and previous studies of the Piedmont by Schroeder et al. 1997; 2000), however, suggest that there is a measurable component of external mineral input.

Long-term fluxes of minerals in the regolith can be evaluated by total mass loss of elements over time. Merritts et al. (1992) have shown that the mass loss (ΔM_j) of an element j can be calculated by integrating τ_i over depth (z). Equation 3 shows the integral form of this relationship in units of moles/ m^2 :

$$\Delta M_j = \left(\rho_p \frac{C_{j,p}}{m_j} 10^4 \right) \int_{z=0}^{z=d} \tau_{j,w} dZ \quad (3)$$

where d is the profile depth, m_j is the molecular mass of species j .

The corresponding mass losses or gains for each oxide are shown in Table 5. If the relative concentrations of the elements are integrated over the saprolitic portion of the profile, then in both cases, there is significant mass loss. This result supports the notion that the majority of chemical mass loss occurs at depth in the regolith. The only exception in the saprolite portion of the profile is the increase in structural water associated with kaolin group mineral formation. The small amount of Fe and Mn increase is likely due to chelated complexes that facilitate transport downward from overlying horizons (Seaman et al. 1997).

When the Elberton profile is integrated over the entire regolith, there is net gain of Si and Al. This is most easily explained by an influx of the elements from wind-blown or fluvial sources and/or as residuals from overlying weathered rocks. Possible sources include: (1) the Elberton Granite itself; (2) residually weathered metamorphic country rock (into which

TABLE 5. Mass losses and gains of major and minor oxides in weathering profiles developed over the Elberton Granite and Shoulderbone schist

Oxide	Elberton Sapolite $\Delta z = 659$ m	Elberton Regolith $\Delta z = 1100$ m	Shoulderbone Sapolite $\Delta z = 101$ m	Shoulderbone Regolith $\Delta z = 170$ m
SiO ₂	-1.7 10 ⁴	2.6 10 ³	-1.0 10 ⁴	-1.3 10 ⁵
Al ₂ O ₃	-1.3 10 ³	4.3 10 ³	-4.7 10 ²	-2.9 10 ²
CaO	-2.2 10 ³	-4.8 10 ³	-5.9 10 ²	-9.3 10 ²
MgO	-2.4 10 ²	-8.5 10 ²	-6.0 10 ³	-7.9 10 ³
Na ₂ O	-3.8 10 ³	-8.9 10 ³	-1.1 10 ²	-1.8 10 ²
K ₂ O	-1.1 10 ³	-1.9 10 ³	-6.0 10 ⁰	-1.5 10 ⁰
Fe ₂ O ₃	1.2 10 ¹	-4.4 10 ¹	-6.9 10 ²	-4.7 10 ²
MnO	1.0 10 ⁰	-2.4 10 ⁰	-3.0 10 ¹	-1.5 10 ¹
P ₂ O ₅	-3.8 10 ¹	-7.9 10 ¹	-1.5 10 ¹	-1.8 10 ¹
Cr ₂ O ₃	-1.5 10 ¹	-1.7 10 ¹	-1.6 10 ¹	-2.0 10 ¹
LOI*	1.4 10 ⁴	4.8 10 ⁵	-3.5 10 ²	2.0 10 ⁵

Notes: Values calculated using Equation 3, assuming TiO₂ is conserved. Units are in moles m⁻². Δz represents the thickness integrated to estimate mass loss.

*Loss on ignition is considered the sum of H₂O and CH₂O (mass gain due to FeO → Fe₂O₃ reaction ignored).

the granitic magma was emplaced); and (3) thin veneers of colluvium and fluvial sediment. The presence of epidote and hornblende in the B-horizon is consistent with a source in the regionally metamorphosed country rocks, because neither has been reported in the granite (Stormer et al. 1980).

The authigenic and ultra-fine (i.e., <1.0 μ m fraction) translocated clay minerals and Fe- and Al oxyhydroxides have clearly modified the bulk mineralogical and chemical characteristics of the A- and B₁-horizons (Table 2). The sand-sized ilmenite in the B₁-horizon has not likely moved through the soil pores. The ilmenite grain population in the A-horizon at Elberton has likely been influenced by quarry operations, which limits interpretation about the source of the grains. The observation of metamorphic components in the upper portion of the soil profile, however, indicates that ilmenite grains near the surface could have multiple origins.

The occurrence of constant ilmenite compositions throughout the profile can be evaluated further by knowing the long-term rate of mass loss in the surrounding Piedmont. This evaluation can only be determined by knowing the duration of weathering and the mass loss. The nearest estimate of Piedmont exposure ages comes from a study of the Panola granite (Schroeder et al. 2001). Based on measurement of the ¹⁰Be and ²⁶Al in near-surface quartz grains at Panola, the surface exposure age is about 125 Ka. Another relevant site is the tropical watershed in Puerto Rico (White et al. 1998). The ΔM_i values in Table 5 for the saprolitic portion of the Elberton are about an order-of-magnitude lower than those measured for weathering of diorite in this tropical watershed. The duration of weathering at the Puerto Rico site is estimated to be about 200 Ka, based on ¹⁰Be accumulations (Brown et al. 1995). If the duration of weathering at the Elberton Granite site is similar to that of the Panola granite, then the long-term weathering flux from this granite in its temperate to subtropical climate is about an order of magnitude less than that measured in tropical climates. At this point in time, there are not enough constraints to know accurately how much residual material is included in the A- and B-horizons at the Elberton site. Integrated cosmogenic nuclide studies could help us make a better comparison and constrain long-term weathering rate estimates.

Local lithologic heterogeneities parallel to the foliation of the Shoulderbone schist increase the likelihood for slight variations in ilmenite abundance. However, the regional metamorphic grade of the Shoulderbone schist is greenschist to amphibolite facies (Biaggi 2002), which suggests that initial ilmenite compositions should be homogeneous. Textural and bulk chemical properties of the schist suggest that, like the Elberton profile, the A- and B₁-horizons at Shoulderbone have undergone chemical modification from overlying allochthonous and residual sources. Table 5 shows mass loss for all components in the saprolitic portion of the profile. When integrated over the entire profile, mass losses are experienced for all components (except for a gain in structural H₂O as implied by the LOI measurement).

This analysis of the bulk-chemical properties, assuming both chemical and physical TiO₂ conservation, reveals that the profiles selected for study may not be entirely residual. Part of the Si, Al enrichment seen in A- and B-horizons of both profiles can be attributed to residua from pre-existing overlying material and additions due to past fluvial, colluvial and eolian processes. With this understanding of overall bulk chemical and mineralogical trends in each profile (rock, saprolite and soil), it is possible to better understand the trends in average ilmenite composition with depth.

Changes in ilmenite properties

Figures 6 and 7 show that the compositions of the Elberton and Shoulderbone ilmenite grains vary as function of position in the horizons. In the case of the Elberton Granite, grains appear enriched in Mn (or depleted in Fe) in the saprolitic horizons as compared with the parent rock and the B-horizon. Texturally, the ilmenite appears to undergo alteration along selective grain boundaries and adjacent to hematite blebs (Fig. 2). Ilmenite grains from the parent rock that contain small hematite blebs appear as having an excess Fe content (Fig. 7c).

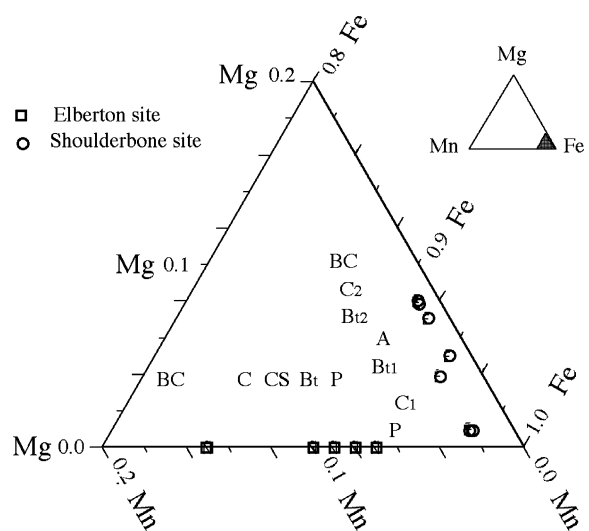
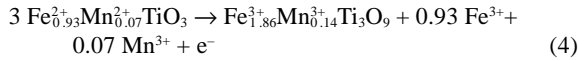


FIGURE 6. Fe-Mg-Mn ternary diagram comparing average composition of Elberton Granite (squares) and Shoulderbone schist ilmenite grains (circles) in the regolith (n = 50 for each data point). See Tables 3 and 4 for other horizon symbol codes.

One reaction that has been proposed to explain the alteration of ilmenite is the anodic oxidation to pseudorutile (Grey and Reid 1975). This reaction mechanism is a solid-state transformation in which Fe^{2+} and Mn^{2+} are oxidized and removed from the rhombohedral structure to produce pseudorutile as an intermediate phase. For ilmenites with compositions similar to those from the Elberton granite, the reaction would appear as follows:



This pathway is commonly observed in beach placer deposits of ilmenite (Babu et al. 1994). Evidence for the solid-state mechanism is not obvious in our XRD patterns. Figure 8 shows that coherent X-ray scatter consistent with the presence of small domains of pseudorutile are barely recognizable.

Secondary phases identified in the Elberton Granite and Shoulderbone schist by XRD and optical microscopy include hematite, goethite, rutile, and anatase (Fig. 8). Formation of these phases is best understood in the context of the following cathodic half-cell reaction between oxygen and water that was concurrent with Reaction 4 and produces hydroxyl groups:

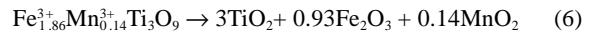


Hydroxyls produced in Reaction 5 can, among other things, readily complex with Fe^{3+} to form goethite.

Oxidation of Mn yields a greater free energy change than oxidation of Fe (Berner 1980) and is therefore more likely to be first utilized by indigenous microbes as an electron source. The trend of increasing Mn content in ilmenite from parent rock to the C-horizon in the Elberton profile may be a consequence of precipitation of nanocrystalline Mn-oxides in ilmenite

micropores that form along high-density lattice nodes. Mn-oxides in soils are commonly reported to be X-ray amorphous, with vernadite ($\delta\text{-MnO}_2$) being the most common variety (McKenzie 1989). Our XRD data also have scatter consistent with the presence of small amounts of the Mn-minerals, groutite and pyrolusite.

The lack of abundant pseudorutile suggests that the intermediate phase transition of ilmenite to pseudorutile is short-lived. This intermediate reaction is promoted by the 6% volume reduction associated with the solid-state transformation (Grey and Reid 1976). Pseudorutile subsequently undergoes incongruent dissolution. This second stage results in precipitation of anatase, rutile, hematite, and Mn oxide as follows:



The reverse trend of decreasing Mn and increasing Fe in ilmenite from the C- to the B-horizon is difficult to explain assuming the profile is entirely residual. One possible mechanism could be the mobilization of MnO_2 from the B- to C-horizon. The bulk Mn content of the soil is the lowest at the B-horizon. Recall, however, that the trends displayed in Figure 8 are only those of the competent ilmenite grains. Many other more highly altered ilmenite grains are present, but their chemistry is not represented in Figure 7. It appears that some of the ilmenite grains in the Elberton profile have been destroyed completely, whereas the others have survived intact. Interestingly, the grains in the B-horizon (and presumably the ilmenite grains that will eventually be part of the sedimentary cycle) have compositions that are statistically indistinguishable from the ilmenite grains in the granite (Le Golvan 2001).

The Shoulderbone ilmenite grains of the B-horizon show a depletion in Fe compared with ilmenites from the parent schist and saprolite (similar to ilmenite from the Elberton granite). In contrast, Mg is enriched in ilmenite found in the B-horizon. Magnesium maintains a constant divalent state under almost all conditions and, therefore, may be responding passively to the effects of Fe oxidation. A reaction pathway similar to the Elberton ilmenite is likely followed by the Shoulderbone il-

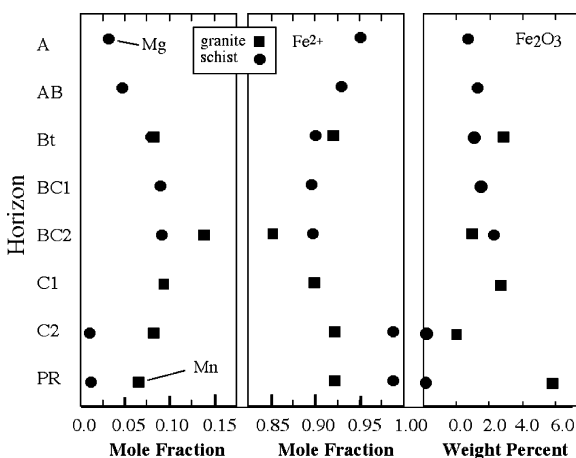


FIGURE 7. Average composition of ilmenite grains as a function of soil horizon position. Manganese is plotted for the Elberton Granite (squares) and Mg is plotted for Shoulderbone schist ilmenite grains (circles) in the left figure. The center figure shows the complimentary values for Fe^{2+} . The right figure plots calculated excess ferrous iron weight percent. Negative values are a consequence of rutile inclusions and the measurement of excess TiO_2 .

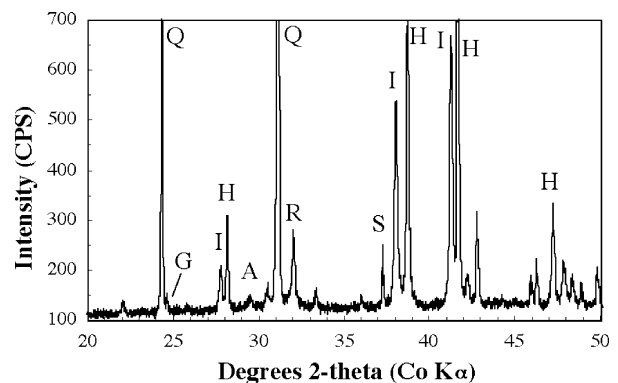
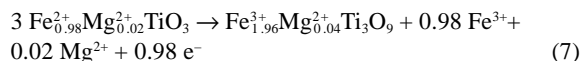


FIGURE 8. XRD patterns of fine-sand Elberton Granite magnetic separates. Selected representative peaks have been labeled to illustrate phases identified. A = anatase, G = goethite/groutite, H = hematite, I = ilmenite, R = rutile, and S = hornblende. Step scanned at $0.01^\circ 2\theta$, with 6 s count time per step.

menite, whereby anodic oxidation occurs during the first step of alteration. Once the limit of lattice stress is reached by solid-state transformation, then an incongruent dissolution-precipitation reaction occurs. The difference between the Elberton and Shoulderbone occurrences is that the Mg at Shoulderbone is partially dissolved and removed by groundwater as in the following half-cell reaction:



A two-population model best explains the increase in Mg content of the ilmenites upward in the Shoulderbone schist profile. Highly fractured grains at Shoulderbone undergo preferential alteration. Grains that are not cracked appear to survive exposure through the various horizons. Microfractured grains show a subtle response to Fe oxidation, as seen in the change in $\text{Fe}^{2+}/\text{Fe}^{3+}$ ratios. Iron oxidation is also supported by optical microscopy, which revealed increased goethite in ilmenite micropores. The calculated hematite component (Table 4) also supports oxidation as the principal alteration mechanism. As explained previously, negative hematite component values for ilmenites from the parent rock and the C-horizon (Fig. 7) could be due to rutile inclusions in the ilmenite grains. The cause of excess Ti seen in some of the analyses results could be better resolved by additional sampling of the parent rock ilmenite compositions. Analyses of ilmenites from C-, B-, and A-horizons above show a significant increase in hematite component, which reflects the formation of goethite and hematite in micropores.

CONCLUDING REMARKS

This investigation of ilmenite in weathering profiles developed on felsic and ultramafic rocks in a temperate to subtropical climate has found distinct textural and chemical alteration trends in the sand-sized population of ilmenite grains. These trends can be ascribed to (1) initial properties inherited from the parent rock; (2) oxidative reactions in A-, B-, and C-horizons; and (3) external inputs into the soil system. Ilmenite minor-element chemistry and grain textures in this study are demonstrably different in felsic and ultramafic host rocks.

Many ilmenite grains in both weathering profiles show a strong oxidation effect and Fe^{2+} depletion in the C-horizon. A two-step reaction mechanism, similar to that proposed by Grey and Reid (1975), seem plausible. Optical, XRD, and chemical data, however, suggest that the pseudorutile is ephemeral. During this weathering stage, Fe and Mn migrate out of the structure and locally precipitate as goethite and MnO_2 . Hematite lamellae are locally recrystallized fine-grained intergrowths as indicated by their reddish color. In acidic soil-weathering profiles, ilmenite appears to undergo both solid-state transformation and dissolution whereby anatase, rutile, hematite, and goethite are precipitated as secondary products. This reaction contrasts with weathered placer beach deposits, where pseudorutile is more abundant and appears to be metastable (Force 1991).

Upward enrichment of Mn in ilmenite from the Elberton C-horizon is attributed to a preferential oxidation and precipita-

tion of Mn. Upward enrichment of Mg in ilmenite from the Shoulderbone C-horizon is attributed to passive concentration resulting from the oxidation of Fe. In all cases, a sub-population of ilmenite grains become altered along either lamellae (Elberton) or grain fractures (Shoulderbone). Another sub-population of competent grains resists alteration and persist in the A- and B-horizons. Bulk-soil composition also suggests that the A- and B-horizons have a component of allochthonous as well as residual material.

In this study, the chemistry of ilmenite grains that would enter sedimentary drainage systems is very similar to that of the parent rock. This finding validates the use of ilmenite minor element chemistry to characterize sedimentary source; however, textures of ilmenite grains may be biased by soil/saprolite weathering processes. Mineral assemblages in the A-horizon also appear to be modified by additions derived from weathered Piedmont metamorphic rocks, and allochthonous components delivered to the site by fluvial, colluvial, and eolian processes.

The utility of ilmenite chemistry and textural properties for petrologic and pedogenic work will only be improved by extending investigations laterally to better understand variability within each rock type. Such studies need to be combined with cosmogenic nuclide studies of regolith components to better constrain the time frame over which ilmenite alteration takes place. The reaction pathways also need to be better understood in the context of microorganisms that are known to accelerate Fe and Mn oxidation in soils.

ACKNOWLEDGMENTS

The NSF—Geologic Record of Global Change Program (EAR9628035) and the University of Georgia Research Foundation, supported this work. The second author expresses thanks to the UGA Watts-Wheeler Fund and The Clay Minerals Society. Larry West and Dixie Hamilton, UGA Crop and Soil Sciences Department, helped with the fieldwork. The comments of Michael Velbel improved the manuscript. The senior author dedicates this paper to Robert (Bob) C. Reynolds and the joy of motorcycles.

REFERENCES CITED

- Anand, R.R. and Gilkes, R.J. (1984) Weathering of ilmenite in a lateritic pallid zone. *Clays and Clay Minerals*, 37, 363–374.
- Babu, D.S.S., Thomas, K.A., Mohan Das, P.N., and Damodaran, A.D. (1994) Alteration of ilmenite in the Manavalakurichi deposit, India. *Clays and Clay Minerals*, 42, 567–571.
- Biaggi, A. (2002) Mineralogy of the Shoulderbone ultramafic body, Hancock County, Georgia, 40 p. B.S. Thesis, University of Georgia, Department of Geology, Athens, Georgia.
- Bailey, S.W., Cameron, E.N., Spedden, H.R., and Weege, R.J. (1956) The alteration of ilmenite in beach sands. *Economic Geology*, 51, 263–279.
- Bastin, G.F., van Loo, F.J.J., and Heijliger, H.J.M. (1984) Evaluation of the Use of Gaussian $\Phi(\rho z)$ Curves in Quantitative Electron Probe Microanalysis: A New Optimization. *X-ray Spectrometry*, 13, 91–97.
- Basu, A. and Molinaroli, E. (1989) Provenance characteristics of detrital opaque Fe-Ti oxide minerals. *Journal of Sedimentary Petrology*, 59, 922–934.
- Berner, R.A. (1980) *Early Diagenesis: A theoretical approach*, 242 p. Princeton University Press, Princeton, N.J.
- Blake, G.R. and Hartge, K.H. (1986) Bulk Density. In A. Klute, Ed., *Methods of Soil Analysis, Part I. Physical and Mineralogical Methods: Agronomy Monograph no. 9* (2nd ed.), 363–375. Soil Science Society of America, Madison, WI.
- Brimhall, G.H. and Dietrich, W.E. (1987) Constitutive mass balance relations between chemical compositions, volume, density, porosity, and strain in metasomatic hydrochemical systems: Results on weathering and pedogenesis. *Geochimica et Cosmochimica Acta*, 51, 567–587.
- Brown, E.T., Stallard, R.F., Larsen, M.C., Raisbeck, G.M., and Yiou, F. (1995) Denudation rates determined from the accumulation of in situ produced ^{10}Be in the Luquillo Experimental Forest, Puerto Rico. *Earth and Planetary Science Letters*, 129, 192–202.
- Buddington, A.F. and Lindsley, D.H. (1964) Iron-titanium oxide minerals and syn-

- thetic equivalents. *Journal of Petrology*, 5, 310–357.
- Chadwick, O.A., Brimhall, G.E., and Hendricks, D.M. (1990) From a black to a gray box—a mass balance interpretation of pedogenesis. *Geomorphology*, 3, 369–390.
- Cornu, S., Lucas, Y., Lebon, E., Ambrosi, J.P., Luizao, F., Rouiller, J., Bonnay, M., and Neal, C. (1999) Evidence of titanium mobility in soil profiles, Manaus, central Amazonia. *Geoderma*, 91, 281–295.
- Darby, D.A. (1984) Trace elements in ilmenite: A way to discriminate provenance or age in coastal sands. *Geological Society of America Bulletin*, 95, 1208–121.
- Darby, D.A. and Tsang, Y.W. (1987) Variation in ilmenite element composition within and among drainage basins: implications for provenance. *Journal of Sedimentary Petrology*, 57, 831–838.
- Deer, W.A., Howie, R.A., and Zussman, J. (1992) *Rock-forming minerals*, 696 p. 2nd edition. Longman Scientific & Technical, Essex, U.K.
- Dimanche, F. and Bartholomé, P. (1976) The alteration of ilmenite in sediments. *Minerals Science Engineering*, 8, 187–200.
- Flinter, B.H. (1959a) The alteration of Malayan ilmenite grains and the question of “Arizonite”. *Economic Geology*, 54, 720–729.
- (1959b) Magnetic separation of some alluvial minerals in Malaya. *American Mineralogist*, 44, 738–751.
- Force, E.R. (1991) Geology of titanium-mineral deposits. *Geological Society of America Special Paper* 259, 112 p.
- Frost, B.R. and Lindsley, D.H. (1992) Equilibria among Fe-Ti oxides, pyroxenes, olivine, and quartz 2 application. *American Mineralogist*, 70, 1004–1020.
- Frost, M.T., Grey, I.E., Harrowfield, I.R., and Mason, K. (1983) The dependence of alumina and silica contents on the extent of alteration of weathered ilmenites from Western Australia. *Mineralogical Magazine*, 47, 201–208.
- Frost, M.T., Grey, I.E., Harrowfield, I.R., and Li, C. (1986) Alteration profiles and impurity element distributions in magnetic fractions of weathered ilmenite. *American Mineralogist*, 71, 167–175.
- Gardner, L.R. (1980) Mobilization of Al and Ti during weathering—iso-volumetric geochemical evidence. *Chemical Geology*, 30, 151–165.
- Grey, I.E. and Reid, A.F. (1975) The structure of pseudorutile and its role in the natural alteration of ilmenite. *American Mineralogist*, 60, 898–906.
- Grigsby, J.D. (1990) Detrital magnetite as a provenance indicator. *Journal of Sedimentary Petrology*, 60, 940–951.
- (1992) Chemical fingerprinting in detrital ilmenite: A viable alternative in provenance research? *Journal of Sedimentary Petrology*, 62, 331–337.
- Haggerty, S. (1976) Opaque mineral oxides in terrestrial igneous rocks. In A. Goresy, S. Haggerty, J.S. Huebner, D.H. Lindsley, and D. Rumble III, Eds., *Oxide Minerals*, 3, 101–301. Short Course Notes, Mineralogical Society of America, Washington, D.C.
- Hamilton-Wood, D.A. (2002) Weathering sequences of contrasting mafic and felsic parent materials in the Georgia Piedmont, U.S., 102 p. M.S. Thesis. University of Georgia, Department of Crop and Soil Science, Athens, Georgia.
- Le Golvan, J.J. (2001) The fate of ilmenite and magnetite in the weathering profile, 162 p. M.S. Thesis. University of Georgia, Department of Geology, Athens, Georgia.
- Lynd, L.E. (1960) Study of the mechanism and rate of ilmenite weathering. *AIME Transactions*, 217, 311–318.
- LeMaitre, R.W. (1976) The chemical variability of some common igneous rocks. *Journal of Petrology*, 17, 589–637.
- McKenzie, R.M. (1989) Manganese oxides and hydroxides. In J.B. Dixon and S.B. Weed, Eds., *Minerals in soil environments* 2nd edition, p. 439–465. Soil Science Society of America, Madison, Wisconsin.
- Merritts, D.J., Chadwick, O.A., Hendricks, D.M., Brimhall, G.H., and Lewis, C.J. (1992) The mass balance of soil evolution on late Quaternary marine terraces, Northern California. *Geological Society of America Bulletin*, 104, 1456–1470.
- Misra, K. and Keller, F.B. (1978) Ultramafic bodies in the southern Appalachians: A review. *American Journal of Science*, 278, 389–418.
- Puffer, J.H. and Cousminer, H.L. (1982) Factors controlling the accumulation of titanium-iron oxide-rich sands in the Cohasset Formation, Lakehurst Area, New Jersey. *Economic Geology*, 77, 379–391.
- Schneiderman, J.S. (1995) Detrital opaque oxides as provenance indicators in River Nile sediments. *Journal of Sedimentary Research*, A65, 668–674.
- Seaman, J.C., Bertsch, P.M., and Strom, R.N. (1997) Characterization of colloids mobilized from southeastern coastal plain sediments. *Environmental Science & Technology*, 31, 2782–2790.
- Schroeder, P.A., Kim, J.G., and Melear, N.D. (1997) Mineralogical and textural criteria for recognizing remnant Cenozoic deposits on the Piedmont: Evidence from Sparta and Greene County, Georgia, U.S.A. *Sedimentary Geology*, 108, 195–206.
- Schroeder, P.A., Melear, N.D., West, L.T., and Hamilton, D.A. (2000) Meta-gabbro weathering in the Georgia Piedmont, USA: Implications for global silicate weathering rates. *Chemical Geology*, 163, 235–245.
- Schroeder, P.A., Melear, N.D., Bierman, P., Kashgarian, M., and Caffee, M.W. (2001) Apparent gibbsite growth ages for regolith in the Georgia Piedmont. *Geochimica et Cosmochimica Acta*, 65, 381–386.
- Stormer, J.C. Jr., Whitney, J.A., and Hess, J.R. (1980) Petrology and geochemistry of the Elberton Granite. In J.C. Stormer Jr. and J.A. Whitney, Eds., *Geological, Geochemical, and Geophysical Studies of the Elberton Batholith, Eastern Georgia*, 19, 10–30. Department of Natural Resources Guidebook, Atlanta, Georgia.
- White, A.F., Blum, A.E., Schultz, M.S., Vivit, D.V., Stonestrom, D.A., Larson, M., Murphy S.F., and Eberl, D. (1998) Chemical weathering in a tropical watershed, Luquillo Mountains, Puerto Rico: I. Long-term versus short-term weathering fluxes. *Geochimica et Cosmochimica Acta*, 62, 209–226.

MANUSCRIPT RECEIVED OCTOBER 30, 2001

MANUSCRIPT ACCEPTED AUGUST 20, 2002

MANUSCRIPT HANDLED BY JAMES ARONSON